THE JOURNAL OF BIOLOGICAL CHEMISTRY
Vol. 280, No. 5, Issue of February 4, pp. 3740–3746, 2005
© 2005 by The American Society for Biochemistry and Molecular Biology, Inc.
Printed in U.S.A.

Crystal Structure of Jun a 1, the Major Cedar Pollen Allergen from *Juniperus ashei*, Reveals a Parallel β-Helical Core*

Received for publication, August 23, 2004, and in revised form, October 29, 2004
Published, JBC Papers in Press, November 10, 2004, DOI 10.1074/jbc.M409655200

Edmund W. Czerwinski‡§, Terumi Midoro-Horiuti¶, Mark A. White‡, Edward G. Brooks¶, and Randall M. Goldblum‡¶

From the ‡Sealy Center for Structural Biology, Department of Human Biological Chemistry and Genetics, University of Texas Medical Branch at Galveston, Galveston, Texas 77555-0647 and the ¶Department of Pediatrics, University of Texas Medical Branch at Galveston, Galveston, Texas, 77555-0366

Pollen from cedar and cypress trees is a major cause of seasonal hypersensitivity in humans in several regions of the Northern Hemisphere. We report the first crystal structure of a cedar allergen, Jun a 1, from the pollen of the mountain cedar *Juniperus ashei* (Cupressaceae). The core of the structure consists primarily of a parallel β-helix, which is nearly identical to that found in the pectin/pectate lyases from several plant pathogenic microorganisms. Four IgE epitopes mapped to the surface of the protein are accessible to the solvent. The conserved vWiDH sequence is covered by the first 30 residues of the N terminus. The potential reactive arginine, analogous to the pectin/pectate lyase reaction site, is accessible to the solvent, but the substrate binding groove is blocked by a histidine-aspartate salt bridge, a glutamine, and an α-helix, all of which are unique to Jun a 1. These observations suggest that steric hindrance in Jun a 1 precludes enzyme activity. The overall results suggest that it is the structure of Jun a 1 that makes it a potent allergen.

Common allergic reactions, including allergic rhinitis and asthma, are initiated when protein or glycoprotein allergens cross-link specific IgE antibody molecules on the surface of mast cells or basophils. However, our understanding of the structural basis of this process is incomplete. For instance, the structures of the receptors that anchor the IgE molecules to cells and the signaling process that ensues after cross-linking are known in some detail. On the other hand, our understanding of the structural requirements for proteins to function as allergens is very limited. It is well known that not all proteins are naturally allergenic, and those that are allergenic belong to a relatively small number of protein families. This suggests that certain structural features or biochemical activities are required for proteins to promote an allergenic response.

We have performed studies of the extremely allergenic glycoproteins from the pollen of the mountain cedar tree, *Juniperus ashei*, a major cause of seasonal hypersensitivity in the central United States (1). The propensity for cedar allergens to induce IgE antibody responses and mediate allergic reactions is indicated by the finding that approximately half of those who suffer from mountain cedar pollinosis do not have reactions to any other allergens. The pollen of related species are responsible for severe, seasonal allergic diseases in Japan (*Cryptomeria japonica* (2, 3) and *Chamaecyparis obtusa* (4)) and Europe (*Cupressus arizonica* (5) and *Cupressus sempervirens* (6)). Furthermore, the pollen from *Juniperus ashei* is cross-reactive with those from other cedars and cypresses (1), suggesting that homologues of the mountain cedar allergen participate in the vigorous allergic responses in diverse geographic regions and human populations.

One of the unresolved questions in immunology is whether the propensity of allergens to induce pathological responses is due to their unique structural features or biochemical activities. Resolving the three-dimensional structures of the cedar allergens and defining their relationship with their biochemical activity and binding to IgE antibodies to form a pathogenic complex on the surface of cells should advance our understanding of the allergic process. In 1999, we isolated and characterized a major mountain cedar allergen, Jun a 1[1] (7), and found it to be a glycoprotein of 346 amino acid residues with a >80% amino acid sequence identity to the group 1 allergens isolated from the Japanese cedar (2, 3), the Japanese cypress (4), the Arizona cypress (5), the Mediterranean Italian cypress (6), and the North American eastern red cedar (*Juniperus virginiana*) (8). This high percentage of sequence identity implies that the group 1 cedar allergens have similar tertiary structures that may be responsible for their allergenicity and the extensive cross-reactivities between the cedar pollen allergens.

Jun a 1 has less extensive sequence identity (20–50%) with the Pel and Pnl of microorganisms. The Pels and Pnls depolymerize the cell walls of plants in the presence of Ca^{2+} ions in a process classically called "maceration" (9, 10). These enzymes injure or destroy fruits by cleaving the α-1,4 glycosidic bond of pectate and pectin, the major components of plant cell walls (11). However, Pnl and Pel are also produced by higher plants where they are thought to promote germination by pollen grains and the ripening (softening) of fruits (12, 13). Despite the relatively low degree of overall sequence identity between

* This research was supported by NICHD, National Institutes of Health-sponsored Child Health Research Center New Project Award Grant P30 HD27841 (to T. M.-H.), NIAID, National Institutes of Health Grant R01 AI052428 (to R. M. G.), funds from the Advanced Technology Program from the Texas Higher Education Coordinating Board (to R. M. G.), funds from the Parker B. Francis Fellowship in Pulmonary Research from the Francis Families Foundation (to T. M.-H.), NIEHS, National Institutes of Health Center Grant P30 ES006676, and funds from the Sealy-Smith Foundation (to E. W. C. and M. A. W.). We declare that we have no competing financial interests. The costs of publication of this article were defrayed in part by the payment of page charges. This article must therefore be hereby marked "*advertisement*" in accordance with 18 U.S.C. Section 1734 solely to indicate this fact.

The atomic coordinates and structure factors (code 1PXZ) have been deposited in the Protein Data Bank, Research Collaboratory for Structural Bioinformatics, Rutgers University, New Brunswick, NJ (http://www.rcsb.org/).

§ To whom correspondence should be addressed. Tel.: 409-772-3287; Fax: 409-747-4745; E-mail: edcz@xray.utmb.edu.

[1] The abbreviations used are: Jun a 1, major allergen from pollen of mountain cedar *Juniperus ashei*; PB, parallel β-helical sheet; Pel, pectate lyase; BsPel, Pnl, pectin lyase.

This paper is available on line at http://www.jbc.org

the microbial and plant Pel, the residue sequences vWiDH and R*XPXX*R (uppercase letters indicate identity residues between enzymes, the v and i indicate conserved residues, and *X* represents any residue) are highly conserved (14). The crystal structures of several Pnl and Pel from the plant microbial pathogens *Aspergillus niger*, *Erwinia chrysanthemi*, and *Bacillus subtilis* have been reported (15–19). None of the crystal structures of the Pnl and Pel have unequivocally identified the vWiDH and R*XPXX*R sequences as being the active sites of the lyases. Scavetta *et al.* (20) calculated the pK_a values for all of the Pel C arginine groups. All except the first arginine in the R*XPXX*R sequence (Arg^{218}) had normal values. The crystal structure of the Pel C indicated that the Arg^{218} was oriented in such a manner to suggest a catalytic role. Scavetta *et al.* (20) modified the Pel C by an R218K mutation that inactivated the pectolytic activity of the enzyme without affecting the tertiary structure of the enzyme. When this mutant Pel C was complexed with a galacturonopentaose oligosaccharide substrate, the crystal structure showed that the substrate bound in a cleft encompassing the R*XPXX*R sequence as well as the postulated Ca^{2+} binding sites (21).

The relationship between the three-dimensional structures of the group 1 cedar pollen allergens and the microbial Pnl and Pel has not been established, because none of the tertiary structures of the cedar pollen allergens had been determined. Our homology modeling studies have suggested that their tertiary structures may be similar (22). However, our pectolytic assays of Jun a 1 and the Jun a 1 homologue from the Japanese cedar pollen, Cry j 1, indicate that there are functional differences. We have not been able to demonstrate pectolytic activity in Jun a 1, and the pectolytic activity of Cry j 1 was very low relative to the Pels from microbial sources.[2] As part of our efforts to explain these observations, we initiated a structural investigation.

We recently reported the crystallization of the Jun a 1 allergen (23). We report here the three-dimensional crystal structure of Jun a 1, the first for a cedar pollen allergen and the first putative plant Pel to be determined. Analysis of the crystal structure revealed that the predominate conformation of Jun a 1 is fundamentally identical to that of the microbial Pnl and Pel. The lack of Pel or Pnl activity of purified Jun a 1 provides an opportunity to investigate the structural requirements for the activity of these enzymes. Furthermore, this is the first report of the structure of a protein isolated from a non-microbial source that contains the parallel β-helical motif.

MATERIALS AND METHODS

Crystallization and Native Data Collection—The Jun a 1 allergen was isolated from mountain cedar pollen (*J. ashei)* collected in northwestern Bexar County, Texas. The allergen was purified using concanavalin A-Sepharose (Amersham Biosciences) chromatography as described previously (7). A preliminary description of the crystallization and preliminary x-ray diffraction data has been published elsewhere (23). In summary, crystals were obtained after 6–7 weeks at 277 K from solutions containing sodium acetate, ammonium acetate, and 23% polyethylene glycol 4000, pH 5.5. The crystals are monoclinic (space group $P2_1$) with four molecules in the unit cell (Table I). All native and heavy atom derivative data were collected from crystals cryoprotected with glycerol and rapidly cooled to 100 K in liquid nitrogen for storage and data collection. A 2.5-Å resolution native data set and heavy atom derivative data sets were collected on a MAC-Science DIP 2030 Image Plate or a Bruker SMART2K charge-coupled device using copper Kα x-rays produced by MacScience M06HF rotating anode generators equipped with Bruker Göbel optics. Image processing and data reduction were performed using DENZO and SCALEPACK from the HKL package (24). A 1.7-Å resolution native data set was collected at the Advanced Photon Source 14-BM-C beamline, λ = 0.9 Å. Data collection statistics of all data sets are summarized in Table I.

Isomorphous Replacement—Heavy atom derivatives were prepared by soaking the native crystals in mother liquor containing the heavy atom reagent K_2PtCl_4 or $UO_2(NO_2)_2$. Data to 2.5-Å resolution from the $PtCl_4^{2-}$ and $UO_2(NO_2)_2$ derivatives were collected as described above for the native 2.5-Å resolution data. The three 2.5-Å resolution data sets were used to solve the structure using the multiple isomorphous replacement procedure in the program SOLVE (25). Four $PtCl_4^{2-}$ sites and four UO_2^{2+} sites were found with a figure of merit of 0.45. Solvent flattening and non-crystallographic symmetry averaging in RESOLVE (25) increased the figure of merit to 0.66.

Phase Improvement and Refinement—The initial Fourier map showed clearly the two molecules in the asymmetric unit. Many of the side chains were readily identifiable. The preponderance of β-structure was clearly visible, thereby establishing the directionality of the coils. However, the connectivity was not evident, and only about one-third of the residues of the two molecules could be built into the model. The high resolution synchrotron data was not isomorphous with the low resolution data. The phases obtained from the 2.5-Å data were extended to 1.7 Å using the SOLVE/RESOLVE programs after rigid body, positional, and *B*-factor refinements of the 2.5-Å model were made using the program CNS (26). This was followed by several cycles of REFMAC (27)/RESOLVE refinement and automated model building with the figure of merit at each stage being 0.33, 0.59, and 0.74, respectively. A nearly complete model of the Jun a 1 structure was built using XTALVIEW (28). Several cycles of molecular dynamics refinement with simulated annealing using the program CNS were performed and interspersed with model building using XTALVIEW. Further refinement was performed using SHELXL (29) interspersed with model building. The refinement converged at a final *R* of 0.193 and an R_{free} of 0.242 for all data. The final structure consists of 692 amino acid residues in two molecules with 701 water molecules. The refinement statistics are summarized in Table I.

Model Quality—The amino acid geometries, as determined using PROCHECK (30), are normal in each molecule in the asymmetric unit with three exceptions. In each molecule there are two *cis*-proline residues (224 and 231). One tyrosine residue (235) has $\varphi\psi$ angles (~67,-48) that place the residue in the disallowed region of the Ramachandran plot (30). The electron density corresponding to the Pro^{224}, Pro^{231}, and Tyr^{235} residues is unequivocal in each molecule in the asymmetric unit.

All figures were drawn using PyMOL.[3] Solvent accessibility calculations were performed using WhatIF (31).[4] Secondary structure alignments were calculated by the method of Krissinel and Henrick (32, 33).[5]

RESULTS

Overall Structure—Jun a 1 crystallized in the $P2_1$ space group with two molecules of Jun a 1 in the asymmetric unit. The structures of both molecules were refined independently and are virtually identical. The root mean square deviation between 311 (90%) of the Cα atoms of the two molecules is 0.2 Å, whereas 35 residues grouped in the various loops have a root mean square deviation of >1.6 Å. The results and discussion which follow apply equally to both molecules, unless stated otherwise.

Jun a 1 is a single chain polypeptide. The right-handed parallel β-helix is the predominant structural motif (Fig. 1). The parallel β-helix conformation of the Jun a 1 is very similar to those of the Pel and Pnl, for which crystal structures have been published and whose coordinates are available from the Protein Data Bank (16, 17, 19, 21, 34, 35) (Fig. 2). The three parallel β-sheets, PB1 (Fig. 2, *green*), PB2 (*red*), and PB3 (*yellow*), are separated by turns, *i.e.* sequences of residues in random coil conformations of variable lengths. Secondary structural elements are identified as described by Yoder *et al.* (15). Turn T1, usually two residues long, connects PB1 with PB2. T2 (connects PB2 to PB3) and T3 (connects PB3 to PB1 of the next coil) are variable in length. The coils are numbered from the N-terminal end of the parallel β-helix (Fig. 1).

[2] E. Czerwinski, T. Midoro-Horuti, M. White, E. Brooks, and R. Goldblum, unpublished observations.

[3] www.pymol.org.

[4] www.cmbi.kun.nl/gv/servers/WIWWWI/.

[5] www.ebi.ac.uk/msd-srv/ssml/.

TABLE I
Crystallographic data collection and refinement statistics

	Native	Native	K_2PtCl_4	$UO_2(OAc)_2$
X-ray source	APS 14-BM-C	MacScience DIP2030H	MacScience DIP2030H	Bruker CCD
Wavelength (Å)	0.9	1.5418	1.5418	1.5418
Resolution (Å)	1.7	2.5	2.5	2.5
Space Group	$P2_1$	$P2_1$	$P2_1$	$P2_1$
a (Å)	53.6	53.4	53.5	53.6
b (Å)	115.0	113.5	112.9	113.7
c (Å)	73.5	72.4	72.5	72.6
β (°)	95.8	96.4	96.3	96.4
Molecules per a.u.[a]	2	2	2	2
Measured reflections	286,470	108,027	114,672	76,152
Unique reflections	89,001	29,648	29,615	29,989
Redundancy[b]	3.2 (2.0)	3.7 (3.6)	3.9 (3.8)	3.2 (2.4)
Completeness[b] (%)	91.3 (47.3)	99.6 (99.9)	99.9 (100.0)	80.1 (29.4)
I/σ[b]	14.5 (4.1)	14.7 (7.5)	11.6 (5.6)	12.4 (4.1)
R_{sym}[b,c] (%)	5.0 (22.5)	6.6 (19.2)	8.5 (27.4)	6.2 (18.4)
Refinement statistics				
Reflections used	84,532			
R_{cryst}[d]	0.193			
R_{free}[e]	0.241			

	Dimer	Molecule A	Molecule B	Water
Number of atoms	5290	2645	2645	701
Average *B*-factor (Å^2)	19.59	18.27	20.90	33.72
Backbone	16.05	14.88	17.22	
Side chain	23.74	21.99	24.95	
R.M.S.[f] deviation (Å)				
Bond lengths	0.017			
Angle distances	0.025			
Ramachandran analysis (%)				
Most favored	519 (87.7)	257 (86.8)	262 (88.5)	
Allowed	67 (11.3)	37 (12.5)	30 (10.1)	
Generously allowed	4 (0.7)	1 (0.3)	3 (1.0)	
Disallowed	2 (0.3)	1 (0.3)	1 (0.3)	

[a] Asymmetric unit.
[b] Numbers in parentheses are for the highest resolution shell.
[c] $R_{sym} = \sum_i \sum_{hkl} |I_i(hkl) - \langle I(hkl)\rangle| / \sum_{hkl} \langle I(hkl)\rangle$, where $I_i(hkl)$ is the *I*th measured diffraction intensity and $\langle I(hkl)\rangle$ is the mean of the intensity for the Miller index (*hkl*).
[d] $R_{cryst} = \sum_{hkl} ||F_o(hkl)| - |F_c(hkl)|| / \sum_{hkl} |F_o(hkl)|$.
[e] $R_{free} = R_{cryst}$ for a test set of reflections (5%).
[f] Root mean square.

The Jun a 1 β-helix is shaped much like the two sheet β-helix but with a short β-strand instead of random coils connecting the two β-sheets (36), giving the cross-sectional shape of the β-helical core the appearance of an isosceles triangle with PB1 anti-parallel to PB3. PB1, T1, and PB2 are regular in length. The average $\varphi\psi$ angles of the first, (54° and 33°) and second (−91° and 156°) residues in T1 are similar to that of the Pel and Pnl. The result is that the PB2 sheet is pointed in a direction nearly perpendicular to the PB1 sheet. T2 and T3 are less regular in length and planarity and contain all but one of the intra-coil loops. Furthermore, the $\varphi\psi$ angles in PB3 vary widely from coil to coil.

Loops—There are five loops of various types (ζ and Ω) (37), motifs, and lengths extending from the β-helical core. Except for the N- and C-terminal loops, the loops invariably begin and end within T2 (Fig. 1). The Thr^{44}-Ala^{67} loop is an exception, as it begins on coil 1 and ends on coil 2. The closeness of the Cα to Cα distances indicates that the loops do not alter the spatial continuity of the β-helical core.

One loop (Thr^{44}-Ala^{67}) traverses the N-terminal, and one (Ala^{270}-Val^{279}) covers the C-terminal end of the β-helix. These loops preclude the end-to-end binding of other Jun a 1 molecules to the β-helix in the manner described by Richardson and Richardson (38).

Salt Bridges—There are 10 salt bridges in each of the two molecules of Jun a 1 (Fig. 1). Most of these salt bridges are between residues in the parallel β-helix coils and residues in the various loops. Two of the salt bridges are unique to Jun a 1. The salt bridge between Asp^5 in the N-terminal helix-turn-helix loop and His^{165} on T1.5 of the β-helix aids in holding the N-terminal helix-turn-helix loop in place and shields the vWiDH sequence, which is always present in the Pnl and Pel and proposed to be an enzymatically active site (20), from the solvent (Table II). In addition, the salt bridge between Asp^{177} and His^{203} traverses the presumed substrate binding groove in the vicinity of the putative active site Arg^{229}.

Stacks—The Pnl and Pel structures are also characterized by their unique stacks of asparagine, aliphatic, and aromatic residues in the interior of the β-helical core. Similar stacks are found in Jun a 1 in the same relative locations in the interior of the β-helical core (Fig. 1). The aromatic stack of Jun a 1 has a tyrosine in the middle; however, the non-polar character of the interior is maintained by a hydrogen bond between the Oη of Tyr^{245} and the oxygen of Met^{230} (Fig. 3). The significance of this unique interaction for any potential Pel and Pnl activity of Jun a 1 is discussed below.

The asparagine and aliphatic stacks are very similar to those found in the Pel and Pnl. However, there are two serines (Ser^{263} and Ser^{298}) on the C-terminal end of the aliphatic stack with their side chains inside the β-helical core. These two serines interact with the asparagine stack, which is formed by the asparagine usually present as the second residue of T1.4 through T1.10. The second residue in T1 is invariably an Asn, which forms a stack in the interior of the β-helix. The one exception is Asp^{301} of T1.10, which forms a hydrogen bond with the Oγ of Ser^{298}. This arrangement, along with the hydrogen

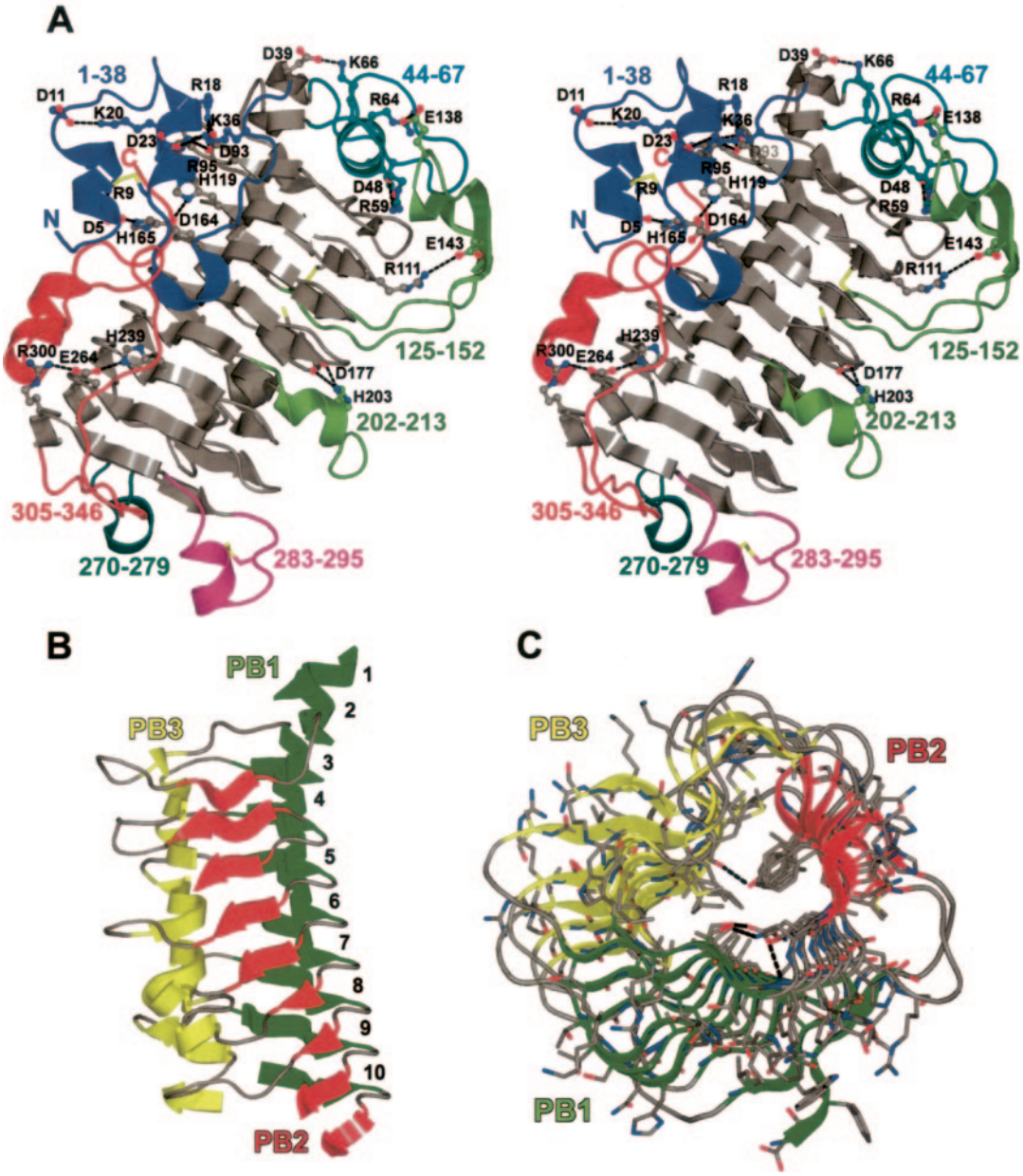

FIG. 1. **Structure of Jun a 1.** *A*, stereo view showing the loops and the salt bridges (*ball and sticks*) we identified. The color of the numbers and the carbon atoms of the salt bridges refer to the loop of the same color. The three disulfides and free sulfhydryl are shown as *sticks* with *black colored* carbons. Single letter amino acid abbreviations are used with position numbers. *B*, parallel β-helical structure of Jun a 1 with loops removed for clarity. Secondary structures are colored as follows: *green*, parallel β-helical sheet PB1; *red*, PB2; *yellow*, PB3. Numbers refer to the PB sheet strand from the N (*top*) to C (*bottom*) termini. *C*, previous figure rotated 90° about the horizontal axis. The view is from the C terminus toward the N terminus of the β-helical core.

bond between Asn^{266} and the Ser^{263} Oγ, maintains the hydrophobic character of the interior of the β-helical core.

Cysteine—The Jun a 1 structure differs from those of the Pnl and Pel structures in the number and placement of the cysteine residues. Jun a 1 has three disulfide bonds and a free sulfhydryl group, whereas the microbial Pels and Pnls have only one or two disulfide bonds in locations different from those in Jun a 1. Furthermore, the Pels and Pnls do not have a free sulfhydryl.

cis-Proline—There are two *cis*-prolines in the Jun a 1 structure, Pro^{224} and Pro^{231}. The *cis*-Pro^{224} residue is in the same locale as the *cis*-Pro^{231} but does not seem to have any unusual interactions as a result of the *cis* configuration. On the other hand, *cis*-Pro^{231} is invariant in the Pnl and Pel. This residue positions the carbonyl oxygen of Met^{230} to form a hydrogen bond with the OH moiety of Tyr^{245}. The electron density map quite clearly shows that the *cis* configuration of Pro^{231} is correct (Fig. 3). There are further ramifications of this configuration, which will be discussed below.

Dihedral Angles—In all of the Pnl and Pel structures published to date, all of the $\varphi\psi$ angles in the polypeptide chains are within the normal limits (30). However, in the Jun a 1 structure the $\varphi\psi$ angles of Tyr^{235} (64° and −48°, respectively) place the residue in the disallowed region of the Ramachandran plot below the left-handed helix region. These $\varphi\psi$ angles create a $\beta_E\gamma$- (or a $\gamma\beta_E$)-type turn (39) between PB3.7 and PB1.8. The only hydrogen bond between the polypeptide backbone nitrogen and oxygen wholly within this β-coil is formed between the Arg^{234} oxygen and the Gly^{236} nitrogen (Fig. 4). As a result, the OH group of Tyr^{235} is positioned to form a hydrogen bond with the 202–213 loop (T3.6).

Proposed Pectolytic Site—The Pnl and Pel contain two highly conserved sequences, vWiDH and R*X*P*XX*R. The biological

function of the vWiDH sequence has not yet been determined with certainty. Non-conserved mutations in this sequence in Pel C produced proteins with pectolytic activity, but these proteins were not well exported and remained associated with the bacterial membrane fraction (40). In Jun a 1, Ala is substituted for Val in position 161 of the conserved vWiDH sequence (161–165). Unlike the Pnl and Pel, the aWiDH sequence of Jun a 1 is covered by a complex loop that extends to the N-terminal end of the β-helical core (Fig. 5).

The R*X*P*XX*R sequence has been shown to be required for Pnl or Pel pectolytic activity (40–43). The crystal structure of a pectolytic inactive mutant of Pel C (R218K), with a plant cell wall fragment complexed to the R*X*P*XX*R sequence of the protein, confirmed this sequence as the pectolytic site (20). Although Jun a 1 does not exhibit pectolytic activity, it does possess the R*X*P*XX*R sequence (229–234), which is located on the side opposite the aWiDH site (Fig. 5). The *cis*-Pro^{231} is strictly conserved, as is Arg^{229}. Residues Arg^{229}, *cis*-Pro^{231}, and Arg^{234} are part of the intricate interactions involving Tyr^{245} in the aromatic stack and Tyr^{235}, which has unfavorable $\varphi\psi$ angles (Fig. 4). The Tyr^{245}-Met^{230}-Tyr^{235} complex appears to fashion the proper environment for Arg^{229} and His^{203}. The *cis*-Pro^{231} is strictly conserved, as is Arg^{229}. Arginine 234 is conserved in the Pel, but in the Pnl the equivalent residue is a glutamine. Although Jun a 1 is not enzymatically active, Arg^{229} is located in the putative enzymatic active site (20, 43) and is also accessible to the solvent (Fig. 6). In addition, the side chain of this putative reactive arginine is extended in the same direction as all of the equivalent arginines in the other Pnl (16, 35) and Pel (17, 19, 21, 34).

Ca^{2+}—Calcium ions are required for pectinolytic activity by the Pels and Pnls. Some of the residues identified as binding to Ca^{2+} and the galacturonopentaose oligosaccharide substrate in the Pel C mutant structure are also in the same spatial arrangement in Jun a 1 (32, 33). However, the two Ca^{2+} binding aspartates (Asp^{160} and Asp^{162}) present in the Pel C are absent in Jun a 1. These two aspartates are part of a loop (152–164) that begins after the vWiDH site and extends into the edge of the active site (Fig. 6, *lower*). This loop is not present in Jun a 1, which reduces the potential for Ca^{2+} binding. Curiously, in Jun a 1 the free sulfhydryl of Cys^{171} is located near to the region where the Pel C loop would begin if it were present. Ser^{196}, Arg^{245}, and Ser^{308} bind to the substrate in Pel C, but in Jun a 1 these residues are His^{203} and Ser^{256}, respectively, and a Ser^{308} equivalent residue is not present. Thus, it is not likely that Jun a 1 would bind Ca^{2+}. In fact the electron density map does not show evidence of Ca^{2+} being present. Furthermore, crystals of Jun a 1 soaked in mother liquor solutions containing high concentrations of Ca^{2+} do not show the presence of Ca^{2+} in the difference electron density maps.

Water—There are 701 water molecules in the crystal structures of the two Jun a 1 molecules. In both of the Jun a 1 molecules in the asymmetric unit there are three waters in the interior of the hydrophobic β-helical core and four waters buried between the helix-loop-helix peptide (residues 1–30) and the aWiDH region (residues 161–165) exterior to the β-helical core. This arrangement adds stability to the association of the N terminus helix-loop-helix moiety with the aWiDH residues, thereby limiting the access of solvent or potential substrates to the aWiDH residues.

IgE Epitopes—The four sites on the Jun a 1 that have been defined as regions to which IgE antibodies bind are on the surface of the molecule (22) (Fig. 7). The backbone portions of these epitopes are part of the β-helix. Epitopes 1–3 are extended on the surface of the β-helix as a part of single rungs and present a linear appearance. Although epitope 4 is composed of the final rung of the β-helix, its C-terminal moiety is part of the random coil structure that extends across the C-terminal end of the β-helix. The result is that epitope 4 presents a more compact surface. The significance of this observation is not clear.

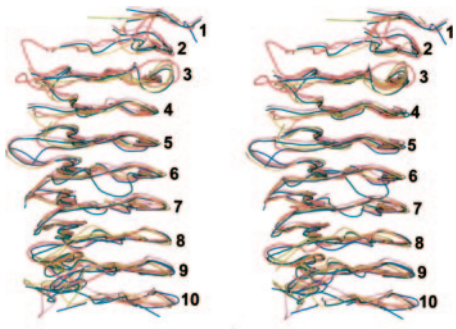

FIG. 2. **Stereo view showing similarity of the β-helical cores of Jun a 1 (*red*) and Pnl A (*turquoise*), Pnl B (*magenta*), Pel A (*orange*), Pel C (*marine*), and *B. subtilis* Pel (*olive*).** The Pels and Pnls are superimposed on the Jun a 1 by their secondary structural elements. Numbers refer to the PB sheet strand from the N (*top*) to C (*bottom*) termini. Orientation is similar to that of Fig. 1*B*.

DISCUSSION

The predominant motif of Jun a 1 is a parallel β-helix. This is the first description of this type of structure in a higher plant or animal. However, many aspects of the Jun a 1 structure are very similar to those of the microbial Pel and Pnl. The similarity in the structures of Jun a 1 and Pel (17, 19, 21, 34) and the Pnl (16, 35) is particularly striking, given the limited amino acid sequence homology. Secondary structure alignments show that the structural similarity between Jun a 1 and the microbial Pnl A and B and the Pel A, C, and *B. subtilis* Pel is concentrated in the β-helical cores, where the differences in the distances between the Cα atoms are <0.7 Å (Fig. 2). Furthermore, the asparagine, aliphatic, and aromatic stacks in the interior of the β-helical core of Jun a 1 are in the same relative

TABLE II
Solvent accessibilities (Å^2) of the vWiDH sequence side chains of Jun a 1 and the pectate lyases

PDB identifier	Type	Ala, Ile, or Val	Trp	Ile or Val	Asp	His
1PXZ	Jun a 1[a]	0.17	0.00	0.52	0	0.17
1BN8	BsPel[b]	0	5.59	0	0.42	5.27
1IDK	Pnl A[c]	0	2.78	0	0.67	4.33
1JTA	Pel A[d]	0	3.49	0.87	0.17	3.29
1QCX	Pnl B[c]	0	3.48	0.17	0.98	12.53
1AIR	Pel C[d]	0	14.85	0	0.63	0.87
1PCL	Pel E[d,e]	13.98	13.80	14.68	11.71	8.04

[a] Source organism, *Juniperus ashei*.
[b] Source organism, *Bacillus subtilis*.
[c] Source organism, *Aspergillus niger*.
[d] Source organism, *Erwinia chrysanthemi*.
[e] 1PCL Pel E structure is Cα only.

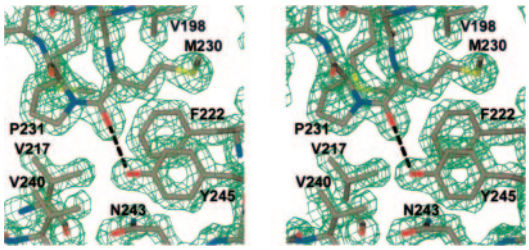

FIG. 3. **Stereo view of the $2F_o - F_c$ map of the β-helical strand (PB3.7-PB2.8) showing the *cis*-Pro^{231} configuration and the internal hydrogen bond (*black dashed line*) between Tyr^{245} and Met^{230} positioned by the *cis*-Pro^{231}.** Also shown are residues of the aliphatic stack (Val^{217} and Val^{240}), the asparagine stack (Asn^{243}), and the aromatic stack (Phe^{222} and Tyr^{245}). Electron density is contoured at the 2 σ level. Single letter amino acid abbreviations are used with position numbers.

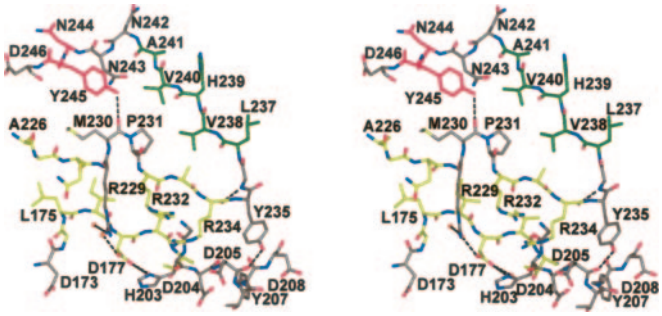

FIG. 4. **Stereo view of residues around the putative pectolytic site (Asp^{177}, His^{203}, Arg^{229}), showing its relationship with the Tyr^{245}-*cis*-Pro^{231} interaction.** Carbon atoms are colored to correspond to the β-pleated sheets (PB3.5, T3.6, PB3.7-PB2.8) depicted in Fig. 1. Single letter amino acid abbreviations are used with position numbers.

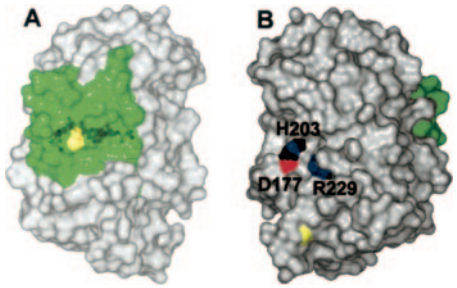

FIG. 5. **The surface of Jun a 1 showing the locations of the R*X*P*XX*R and aWiDH sites.** *A*, the aWiDH residues covered by residues 1–30 (*green*). *Yellow* depicts the disulfide bond between Cys^7 and Cys^{27}. *B*, view of *panel A* rotated 90° about the vertical axis showing the potential substrate binding groove around the active site. His^{203} (*H203*) and Arg^{229} (*R229*) are shown in Corey-Pauling-Koltun colors. *Yellow* depicts the disulfide bond between Cys^{285} and Cys^{291}. The aWiDH site is the *green area* on the *right*. *D177*, Asp^{177}.

locations as those of the Pnl and Pel structures (Fig. 1). In contrast, differences in the distances between the Cα atoms that are not in the β-helical core are >1.8 Å, largely because the positions and conformations of the loops of Jun a 1 are quite different from those of the Pnl and Pel loops. This could explain the differences in biological activities between Jun a 1 and the microbial Pnl and Pel enzymes. Such differences could also explain the differences in allergenicity between Jun a 1 and its homologues from other plants (1).

Secondary structure alignments of the microbial Pel and Pnl indicate that the invariant vWiDH sequence is located in a similar region of Jun a 1. However, the aWiDH sequence is covered by a helix-turn-helix moiety not found in the microbial Pel and Pnl. Furthermore, solvent accessibility calculations indicate that unlike their counterparts in the microbial Pnl and

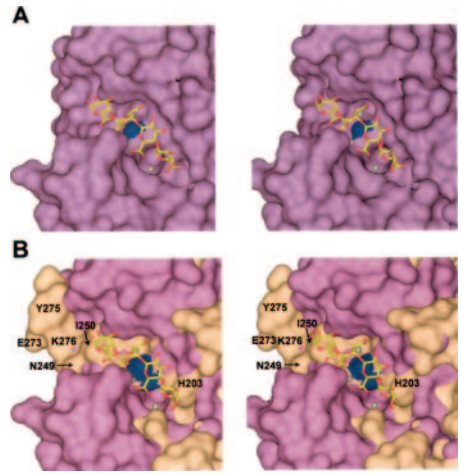

FIG. 6. **The surfaces of Jun a 1 (*wheat*) aligned with the R218K mutant of Pel C (*violet*) according to the secondary structural elements.** *A*, surface view of the pectolytic site of the Pel C mutant with the tetragalactouronate (*yellow sticks*, carbons) and Ca^{2+} ions (*light gray spheres*). *Blue* shows the nitrogen surface of the Lys^{218} Nζ. The surfaces of residues in this area unique to Jun a 1 are not shown. *B*, same view as in *panel A* with the surfaces of the residues unique to Jun a 1 included. The nitrogen surfaces of Arg^{229} of Jun a 1 are shown in *blue*. Lys^{197} is located to the left of Arg^{229} but is not visible in this view. Note that the nonreducing end of the substrate would have to be positioned within the ring of His^{203} if it were to bind to Jun a 1. Single letter amino acid abbreviations are used with position numbers.

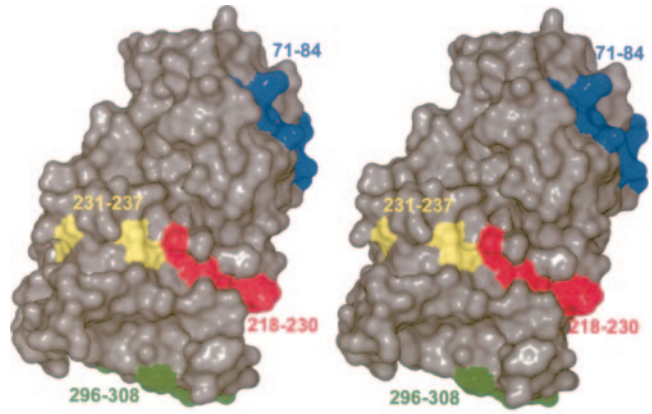

FIG. 7. **Stereo view showing the location of the epitopes.** The view is the same as in Fig. 1*A*.

Pel, the aWiDH residues are not accessible to the solvent (Table II and Fig. 5). It is interesting to note that the Jun a 1 sequence of the helix-turn-helix moiety is ~90% conserved in the Pel of the higher plants. Whether or not the covering of the aWiDH region is a feature common to the higher plants and is an inhibitor of an as yet unidentified biological activity are matters for future investigation.

The invariant sequence of R*X*P*XX*(R/Q), which has been shown to be required for Pnl or Pel activity (40), is also present in Jun a 1 as well as the other plant Pel-like molecules that have been sequenced. The R*X*P*XX*R active sites of the microbial Pnl and Pel are in an unobstructed cleft (Fig. 6*A*). Because the natural substrate is a polysaccharide embedded in a plant cell wall, it follows that a large linear space on the surface is required, as is seen for Pel C and the R218K Pel C mutant. None of the crystal structures of the Pnl and Pel indicate any interactions across the cleft, which could disrupt the concavity of the region.

The equivalent region in Jun a 1 is not as open (Fig. 6*B*). A comparison of Fig. 6, *A* and *B* clearly shows that the galacturonopentaose substrate cannot fit into the Jun a 1 active site.

Not only does the His^{203} side chain occupy the area where the non-reducing terminus of the substrate would bind, but Lys^{197}, Asn^{249}, and Ile^{250} would also interfere with substrate binding, as would Glu^{273} and Tyr^{275} located further along the cavity. Clearly, steric hindrance is the primary reason for the lack of pectolytic activity by Jun a 1.

Homology modeling studies predicted that the four linear IgE epitopes we identified for Jun a 1 would be on the surface of the molecule and accessible to the solvent (22). The three-dimensional structure of Jun a 1 described here confirmed the location of the four linear epitopes on the surface of the molecule. The finding that the Jun a 1 epitopes are part of the β-helical core of Jun a 1 challenges the concept that epitopes are often located in more flexible regions of the allergens. Furthermore, the Jun a 1 structural and enzymatic activity data indicate that pectolytic activity is not a determinant of the allergenicity of the group I plant allergens, nor do these data exclude a role for some unknown biological activity of Jun a 1 and its plant homologues. The structural analysis of Jun a 1 reported here also suggests that both the gross molecular conformation and fine structures of the Pel and Pnl enzymatic sites are highly conserved in plant molecules, although their biological functions remain to be elucidated.

Acknowledgment—We are grateful to Prof. F. Jurnak, University of California, Irvine, for the coordinates of the Pel C R218K mutant complexed with galacturonopentaose as a plant cell wall fragment.

REFERENCES

1. Schwietz, L. A., Goetz, D. W., Whisman, B. A., and Reid, M. J. (2000) *Ann. Allergy Asthma Immunol.* **84,** 87–93
2. Sato, K., Nakazawa, T., Sahashi, N., and Kochibe, N. (1997) *Ann. Allergy Asthma Immunol.* **79,** 57–61
3. Sone, T., Komiyama, N., Shimizu, K., Kusakabe, T., Morikubo, K., and Kino, K. (1994) *Biochem. Biophys. Res. Commun.* **199,** 619–625
4. Suzuki, M., Komiyama, N., Itoh, M., Itoh, H., Sone, T., Kino, K., Takagi, I., and Ohta, N. (1996) *Mol. Immunol.* **33,** 451–460
5. Aceituno, E., Del Pozo, V., Minguez, A., Arrieta, I., Cortegano, I., Cardaba, B., Gallardo, S., Rojo, M., Palomino, P., and Lahoz, C. (2000) *Clin. Exp. Allergy* **30,** 1750–1758
6. Ford, S. A., Baldo, B. A., Panzani, R., and Bass, D. (1991) *Int. Arch. Allergy Appl. Immunol.* **95,** 178–183
7. Midoro-Horiuti, T., Goldblum, R. M., Kurosky, A., Goetz, D. W., and Brooks, E. G. (1999) *J. Allergy Clin. Immunol.* **104,** 608–612
8. Midoro-Horiuti, T., Goldblum, R. M., and Brooks, E. G. (2001) *Clin. Exp. Allergy* **31,** 771–778
9. Barras, F., Vangijsegem, F., and Chatterjee, A. K. (1994) *Annu. Rev. Phytopathol.* **32,** 201–234
10. Collmer, A., and Keen, N. T. (1986) *Annu. Rev. Phytopathol.* **24,** 383–409
11. Pilnik, W., and Rombouts, F. M. (1981) in *Enzymes and Food Processing* (Birch, G. G., Blakebrough, N., and Parker, K. J., eds), pp. 105–128, Applied Science Publishers Ltd., London
12. Carpita, N., and McCann, M. (2000) in *Biochemistry and Molecular Biology of Plants* (Buchanan, B. B., Gruissem, W., and Jones, R. L., eds), pp. 52–108, American Society of Plant Physiologists, Rockville, MD
13. Marin-Rodriguez, M. C., Smith, D. L., Manning, K., Orchard, J., and Seymour, G. B. (2003) *Plant Mol. Biol.* **51,** 851–857
14. Midoro-Horiuti, T., Goldblum, R. M., Kurosky, A., Wood, T. G., Schein, C. H., and Brooks, E. G. (1999) *J. Allergy Clin. Immunol.* **104,** 613–617
15. Yoder, M. D., Lietzke, S. E., and Jurnak, F. (1993) *Structure* **1,** 241–251
16. Mayans, O., Scott, M., Connerton, I., Gravesen, T., Benen, J., Visser, J., Pickersgill, R., and Jenkins, J. (1997) *Structure* **5,** 677–689
17. Thomas, L. M., Doan, C. N., Oliver, R. L., and Yoder, M. D. (2002) *Acta Crystallogr. Sect. D Biol. Crystallogr.* **58,** 1008–1015
18. Akita, M., Suzuki, A., Kobayashi, T., Ito, S., and Yamane, T. (2001) *Acta Crystallogr. Sect. D Biol. Crystallogr.* **57,** 1786–1792
19. Pickersgill, R., Jenkins, J., Harris, G., Nasser, W., and Robert-Baudouy, J. (1994) *Nat. Struct. Biol.* **1,** 717–723
20. Scavetta, R. D., Herron, S. R., Hotchkiss, A. T., Kita, N., Keen, N. T., Benen, J. A., Kester, H. C., Visser, J., and Jurnak, F. (1999) *Plant Cell* **11,** 1081–1092
21. Yoder, M. D., Keen, N. T., and Jurnak, F. (1993) *Science* **260,** 1503–1507
22. Midoro-Horiuti, T., Mathura, V., Schein, C. H., Braun, W., Yu, S., Watanabe, M., Lee, J. C., Brooks, E. G., and Goldblum, R. M. (2003) *Mol. Immunol.* **40,** 555–562
23. Liu, D., Midoro-Horiuti, T., White, M. A., Brooks, E. G., Goldblum, R. M., and Czerwinski, E. W. (2003) *Acta Crystallogr. Sect. D Biol. Crystallogr.* **59,** 1052–1054
24. Otwinowski, Z., and Minor, W. (1997) *Methods Enzymol.* **276,** 307–326
25. Terwilliger, T. C., and Berendzen, J. (1999) *Acta Crystallogr. Sect. D Biol. Crystallogr.* **55,** 849–861
26. Brunger, A. T., Adams, P. D., Clore, G. M., DeLano, W. L., Gros, P., Grosse-Kunstleve, R. W., Jiang, J. S., Kuszewski, J., Nilges, M., Pannu, N. S., Read, R. J., Rice, L. M., Simonson, T., and Warren, G. L. (1998) *Acta Crystallogr. Sect. D Biol. Crystallogr.* **54,** 905–921
27. Collaborative Computational Project No. 4 (1994) *Acta Crystallogr. Sect. D Biol. Crystallogr.* **50,** 760–763
28. McRee, D. E. (1999) *J. Struct. Biol.* **125,** 156–165
29. Sheldrick, G. M., and Schneider, T. R. (1997) in *Methods in Enzymology: Macromoecular Crystallography, Part B* (Carter, J., C.W., and Sweet, R. M., eds) Vol. 277, pp. 319–343, Academic Press, San Diego
30. Laskowski, R. A., Rullmannn, J. A., MacArthur, M. W., Kaptein, R., and Thornton, J. M. (1996) *J. Biomol. NMR* **8,** 477–486
31. Rodriguez, R., Chinea, G., Lopez, N., Pons, T., and Vriend, G. (1998) *Comput. Appl. Biosci.* **14,** 523–528
32. Krissinel, E., and Henrick, K. (2003) in *Proceedings of the 5th International Conference on Molecular Structural Biology, Vienna, September 3–7, 2003* (Kungl, A. J., and Kungl, P. J., eds) p. 88, Biochemistry Subgroup of the Austrian Chemical Society, Vienna
33. Boutselakis, H., Dimitropoulos, D., Fillon, J., Golovin, A., Henrick, K., Hussain, A., Ionides, J., John, M., Keller, P. A., Krissinel, E., McNeil, P., Naim, A., Newman, R., Oldfield, T., Pineda, J., Rachedi, A., Copeland, J., Sitnov, A., Sobhany, S., Suarez-Uruena, A., Swaminathan, J., Tagari, M., Tate, J., Tromm, S., Velankar, S., and Vranken, W. (2003) *Nucleic Acids Res.* **31,** 458–462
34. Lietzke, S. E., Yoder, M. D., Keen, N. T., and Jurnak, F. (1994) *Plant Physiol.* **106,** 849–862
35. Vitali, J., Schick, B., Kester, H. C., Visser, J., and Jurnak, F. (1998) *Plant Physiol.* **116,** 69–80
36. Brèandāen, C.-I., and Tooze, J. (1999) *Introduction to Protein Structure*, 2nd Ed., pp. 84–86 Garland Publishing, New York
37. Ring, C. S., Kneller, D. G., Langridge, R., and Cohen, F. E. (1992) *J. Mol. Biol.* **224,** 685–699
38. Richardson, J. S., and Richardson, D. C. (2002) *Proc. Natl. Acad. Sci. U. S. A.* **99,** 2754–2759
39. Wilmot, C. M., and Thornton, J. M. (1990) *Protein Eng.* **3,** 479–493
40. Kita, N., Boyd, C. M., Garrett, M. R., Jurnak, F., and Keen, N. T. (1996) *J. Biol. Chem.* **271,** 26529–26535
41. Herron, S. R., Benen, J. A., Scavetta, R. D., Visser, J., and Jurnak, F. (2000) *Proc. Natl. Acad. Sci. U. S. A.* **97,** 8762–8769
42. Henrissat, B., Heffron, S. E., Yoder, M. D., Lietzke, S. E., and Jurnak, F. (1995) *Plant Physiol.* **107,** 963–976
43. Lietzke, S. E., Scavetta, R. D., Yoder, M. D., and Jurnak, F. (1996) *Plant Physiol.* **111,** 73–92